



# CHORUS

This is the accepted manuscript made available via CHORUS. The article has been published as:

## Asymmetric couplings enhance the transition from chimera state to synchronization

Changhai Tian, Hongjie Bi, Xiyun Zhang, Shuguang Guan, and Zonghua Liu

Phys. Rev. E **96**, 052209 — Published 14 November 2017

DOI: [10.1103/PhysRevE.96.052209](https://doi.org/10.1103/PhysRevE.96.052209)

# Asymmetric couplings enhance the transition from chimera state to synchronization

Changhai Tian,<sup>1,2</sup> Hongjie Bi,<sup>1</sup> Xiyun Zhang,<sup>1</sup> Shuguang Guan,<sup>1</sup> and Zonghua Liu<sup>1,\*</sup>

<sup>1</sup>*Department of Physics, East China Normal University, Shanghai, 200062, P. R. China*

<sup>2</sup>*School of Data Science, Tongren University, Tongren 554300, P. R. China*

(Dated: November 3, 2017)

Chimera state has been well studied recently, but little attention has been paid to its transition to synchronization. We here study this topic by considering two groups of adaptively coupled Kuramoto oscillators. By searching the final states of different initial conditions, we find that the system can easily show a chimera state with robustness to initial conditions, in contrast to the sensitive dependence of chimera state on initial conditions in previous studies. Further, we show that in the case of symmetric couplings, the behaviours of the two groups are always complementary each other, i.e. robustness of chimera state, except a small basin of synchronization. Interestingly, we reveal that the basin of synchronization will be significantly increased when either the coupling of inner groups or that of inter-groups are asymmetric. This transition from the attractor of chimera state to the attractor of synchronization is closely related to both the phase delay and the asymmetric degree of coupling strengths, resulting in a diversity of attractor's patterns. A theory based on the Ott-Antonsen ansatz is given to explain the numerical simulations. This finding may be meaningful for the control of competition between two attractors in biological systems such as the cardiac rhythm and ventricular fibrillation etc.

PACS numbers:

## I. INTRODUCTION

The collective behaviors of coupled oscillators, especially those on complex networks, have been intensively studied in the fields of both nonlinear science and complex networks for a long time and most of the attentions has been paid to the synchronization [1–5]. It is now well known that the synchronization on complex networks can be seriously influenced by network topologies such as the small world network [6, 7], scale-free networks [8, 9], weighted networks [10, 11], and multi-layered networks [12, 13] etc. In recent years, a new kind of partial synchronization, called chimera state (CS), have been discovered and accordingly, a lot of attentions have been focused on it.

CS was first noticed by Kuramoto and Battogtokh in non-locally coupled identical oscillators in 2002 [14] and then named as *Chimera State* by Abrams and Strogatz in 2004 [15]. It is a kind of coexistence of coherent and incoherent behaviors in the system of identical oscillators from judicious chosen initial conditions and thus depends sensitively on the asymmetric distribution of initial conditions. After that, CS has attracted a lot of attention in the past decade [16–28] and has been successfully used to explain the phenomenon of uni-hemispheric sleep of many creatures in real world such as dolphin, birds, some aquatic mammals, and reptiles etc [29–33]. So far, CS has been extended to the case of nonlocally coupled oscillators where its sensitive dependence on initial conditions is significantly reduced. In this way, one can expect CS in different systems such as the neural systems [34–38], chaotic systems [39–41], high dimensional systems [19, 42–46] and even experimental systems [47–54] etc.

Although these great achievements, little attention has been paid to the transition from CS to synchronization. If we con-

sider CS and synchronization as two attractors, the transition between them represents a competition, which can be expected in many biological systems. For examples, in the heart, there is a competition between the normal rhythmic activity and cardiac fibrillation [55–57]. In the neocortex, there is a competition between the down state (resting state) and up state (state of depolarization) [58–60]. Thus, it is very necessary to study the transition between CS and synchronization.

In this paper, we present an adaptive model of CS to study the transition between CS and synchronization, which consists of two groups of adaptively coupled Kuramoto oscillators. By this model we show that its CS has robustness to initial conditions, in contrast to the sensitive dependence of CS on initial conditions in previous studies. On the other hand, according to the best of our knowledge, most studies of CS are focused on the case of symmetric couplings. Thus, it is unclear what will happen if the couplings are asymmetric. To figure out the answer, we here focus on the influence of asymmetric couplings on CS. We find that the basin of synchronization is very small when the couplings are symmetric in both the inner and inter-groups. However, the basin of synchronization will be significantly increased and accordingly, the basin of CS will be decreased, when either the couplings of inner groups or that of inter-groups become asymmetric. A theoretical analysis based on the Ott-Antonsen ansatz is presented to explain the numerical results. We also find that this transition can be influenced by both the phase delay and the asymmetric degree of coupling strengths.

The paper is organized as follows. In Sec.II, we introduce the adaptive model of CS and numerically study its collective behaviors. In Sec.III, we make a theoretical analysis and a comparison with the numerical simulations. Finally, in Sec. IV, we give conclusions and discussions.

---

\*Electronic address: zhliu@phy.ecnu.edu.cn

## II. THE ADAPTIVE MODEL OF CS AND ITS NUMERICAL SIMULATIONS

We consider a model of two groups of coupled identical oscillators, defined as

$$\begin{aligned}\dot{\theta}_{i,a} &= \omega + \frac{R_a c_{aa}}{N} \sum_{j=1}^N \sin(\theta_{j,a} - \theta_{i,a} - \alpha) \\ &\quad + \frac{R_a c_{ab}}{N} \sum_{j=1}^N \sin(\theta_{j,b} - \theta_{i,a} - \alpha), \\ \dot{\theta}_{i,b} &= \omega + \frac{R_b c_{bb}}{N} \sum_{j=1}^N \sin(\theta_{j,b} - \theta_{i,b} - \alpha) \\ &\quad + \frac{R_b c_{ba}}{N} \sum_{j=1}^N \sin(\theta_{j,a} - \theta_{i,b} - \alpha),\end{aligned}\quad (1)$$

where  $a$  and  $b$  represent the two groups, respectively, and  $i = 1, \dots, N$  represents the  $N$  oscillators in each group. The oscillators are globally coupled with coupling strengths  $c_{aa}$  and  $c_{bb}$  in the groups  $a$  and  $b$ , respectively, and coupling strengths  $c_{ab}$  and  $c_{ba}$  between the two groups, respectively.  $\alpha$  is a phase lag parameter. If there is no special explanation, we set  $\alpha$  as  $\alpha = \frac{\pi}{2} - 0.1$ , which was chosen by many CS papers [31–33]. The couplings are attractive when  $\alpha < \pi/2$  and repulsive when  $\alpha > \pi/2$ .

The parameters  $R_a$  and  $R_b$  represent the order parameters in the groups  $a$  and  $b$ , respectively, and are defined as

$$R_a e^{i\Phi_a} = \frac{1}{N} \sum_{j=1}^N e^{i\theta_{j,a}}, \quad R_b e^{i\Phi_b} = \frac{1}{N} \sum_{j=1}^N e^{i\theta_{j,b}}. \quad (2)$$

where  $\Phi_a$  and  $\Phi_b$  denote the average phases in the groups  $a$  and  $b$ , respectively. From this definition we see that the coupling strength of each group is controlled by their individual local order parameters  $R_a$  and  $R_b$ , respectively. Thus, the coupling strengths are closely correlated to their local coherence and can be regarded as adaptive couplings. This kind of adaptive coupling was addressed in Refs. [13, 61], where the oscillators were considered to be nonidentical with  $\omega_i$  satisfying a distribution and the purpose was to study the explosive synchronization. But we here consider the case of identical oscillators and focus on the transition between CS and synchronization. In fact, the adaptive control is a key topic in the field of engineering control. Thus, the model (1) with adaptive local order parameters may provide new insights to the field of engineering control.

Firstly, we consider the case of symmetric coupling, i.e.  $c_{aa} = c_{bb}$  and  $c_{ab} = c_{ba}$ . We take the initial phases of Eq. (1) from the circular Cauchy distribution [62]

$$g(\theta(0)) = \frac{1 - |\gamma|^2}{2\pi |e^{i\theta} - \gamma|^2} \quad (3)$$

which can be easily generated from a Lorentzian distribution  $g(x) = \frac{1}{\pi} [\frac{\eta}{(x-x_0)^2 + \eta^2}]$  with  $\eta$  being the half width at half

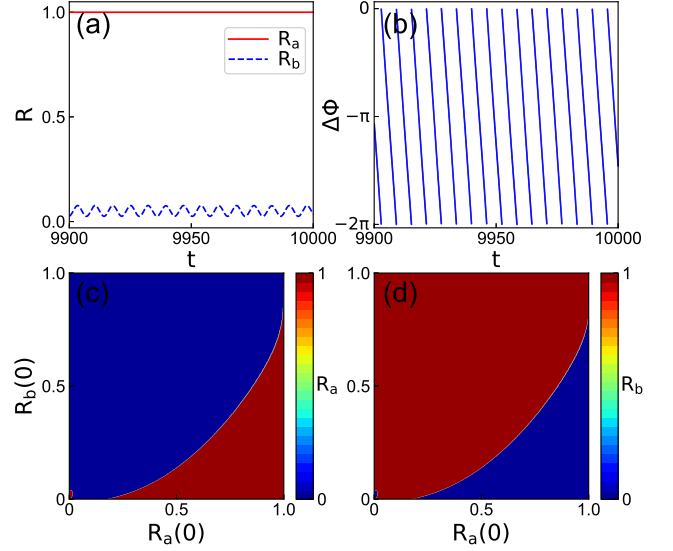


FIG. 1: (color online). (a) and (b) represent the stationary state of CS for a specific distribution of initial conditions with  $R_a(0) = 0.8214$ ,  $R_b(0) = 0.1087$  and  $\Delta\Phi(0) = \Phi_a(0) - \Phi_b(0) = \frac{\pi}{4}$ . (a) The dashed blue and solid red lines denote the  $R_a$  and  $R_b$ , respectively. (b)  $\Delta\Phi(t)$  versus  $t$ . (c) and (d) represent the values of averaged  $R_a$  and  $R_b$  in the phase diagrams of initial conditions, respectively, with the initial phase difference fixed at  $\Delta\Phi(0) = \frac{\pi}{4}$ .

maximum and  $x_0$  being the center of the distribution. Making a transformation  $X = \frac{x+i}{x-i}$ , we can get a new complex variable  $X$ , which is distributed on a unit circular in complex plane. The phases of  $X$  are distributed as the circular Cauchy distribution. By changing  $x_0$  and  $\eta$ , we can easily change the average and deviation of the circular Cauchy distribution and thus change the initial order parameter of the oscillators.

In numerical simulations, we take the system size as  $N = 50$  for each group and let  $c_{aa} = c_{bb} = 1.0$  and  $c_{ab} = c_{ba} = 1.0$ . Without loss of generality, we let the natural frequency  $\omega$  in Eq. (1) be zero. We find that CS can be easily observed in the system of Eq. (1). Fig. 1(a) shows the dependence of  $R_a$  and  $R_b$  on time  $t$  in stationary state, where the initial order parameters are chosen as  $R_a(0) = 0.8214$  and  $R_b(0) = 0.1087$ . We see that  $R_a$  is always unity while  $R_b$  is much smaller than unity, indicating that the oscillators in group  $a$  are synchronized while that in group  $b$  are not synchronized, i.e. the feature of CS. Further, we let  $\Delta\Phi(t) \equiv \Phi_a(t) - \Phi_b(t)$  be the average phase difference between the two groups. Fig. 1(b) shows the dependence of  $\Delta\Phi(t)$  on time  $t$ , corresponding to Fig. 1(a). It is easy to see that  $\Delta\Phi(t)$  is in oscillatory, confirming the difference of states between the groups  $a$  and  $b$ .

It has been pointed out that CS depends sensitively on the distribution of initial conditions [31, 33]. Thus, to successfully observe CS, one has to carefully choose the initial conditions. However, we here surprisingly find that the CS in Eq. (1) does not depend sensitively on its initial conditions, i.e. the adaptive model of Eq. (1) has robustness to initial conditions. Fig. 1(c) and (d) show the dependence of the averaged

order parameters  $R_a$  and  $R_b$  of the two groups on different initial order parameters  $R_a(0)$  and  $R_b(0)$ , respectively, where the initial phase difference between the two groups is fixed as  $\Delta\Phi(0) = \Phi_a(0) - \Phi_b(0) = \frac{\pi}{4}$ . Comparing the corresponding regions between Fig. 1(c) and Fig. 1(d), we see that  $R_a$  will be unity once  $R_b$  is around zero, and vice versa, indicating the CS of the system (1). We also notice that the collective behaviours of the two groups are almost always complementary each other, implying that its CS is robust to initial conditions, i.e. a robustness of CS.

We may notice from Fig. 1(a) that  $R_a$  is a constant 1, while the value of  $R_b$  in the group  $b$  is not only small but also oscillatory. To understand it in detail, Fig. 2(a) shows the effective frequencies  $\langle\dot{\theta}_i\rangle$  and the instantaneous frequencies  $\dot{\theta}_i(t)$  by the red “squares” and green “points”, respectively. We see that in the group  $a$  with  $i \in [1, 50]$ , both  $\langle\dot{\theta}_i\rangle$  and  $\dot{\theta}_i(t)$  are constants around  $-1$  but with a small difference. While in the group  $b$  with  $i \in [51, 100]$ ,  $\langle\dot{\theta}_i\rangle$  is a constant 0 but  $\dot{\theta}_i(t)$  are different for different oscillators and are well organized into a smooth curve. Fig. 2(b) and (c) show the evolutions of  $\dot{\theta}_i(t)$  for the groups  $a$  and  $b$ , respectively. From Fig. 2(b) we see that  $\dot{\theta}_i(t)$  are synchronized and periodically changed with  $t$  between  $-1.04$  and  $-0.98$ , resulting in  $\langle\dot{\theta}_i\rangle = -1.01$  for the group  $a$ . From Fig. 2(c) we see that  $\dot{\theta}_i(t)$  are unsynchronized but formed a traveling wave with amplitudes  $\pm 0.04$ , resulting in  $\langle\dot{\theta}_i\rangle = 0$  for the group  $b$ . Combining Fig. 2(a) with (c) together, we see that they are exactly the Bellerophon state with synchronized average frequencies but unsynchronized instantaneous frequencies, i.e. a phenomenon discovered in non-identical oscillators [63–65].

We have to point out that this is the first time to observe the Bellerophon state in populations of identical oscillators. This finding forces us to pay more attention on the CS in Fig. 1(c) and (d). By carefully checking their behaviours, we interestingly find that they are not always complementary each other, but have a small probability for the two groups to be synchronized. For conveniently characterizing this phenomenon, we follow the Ref. [68] to let “S” denote the attractor of synchronization with  $R_a = R_b = 1$  and “C” the attractor of CS. Fig. 3(a) shows the result in the phase diagram of initial conditions. We see that the region of attractor “S” is very small, but it does exist. Then, a key question is what is the relationship between these two attractors. To go a deeper step toward this question, we change the symmetric couplings in Eq. (1) into asymmetric ones and discuss two kinds of asymmetric couplings in the following.

Secondly, we consider the first kind of asymmetric couplings with  $c_{aa} = c_{bb}$  but  $c_{ab} \neq c_{ba}$ , i.e. non-symmetric inter-group couplings. In numerical simulations, we keep  $c_{aa} = c_{bb} = 1.0$  but take  $c_{ab} = 0.1$  and  $c_{ba} = 1.0$  as an example. We find that the attractor “S” can be enhanced by the asymmetric couplings. Fig. 3(b) shows the result. Comparing Fig. 3(b) with (a) one can see that the region of the attractor “S” is significantly increased. To figure out the answer, we show the phase diagrams of  $R_a$  and  $R_b$  in Fig. 3(c) and (d), respectively. From them we notice two points: (i) The whole region of Fig. 3(d) is synchronized, reminding us the phenomenon of symmetric states requiring system asymme-

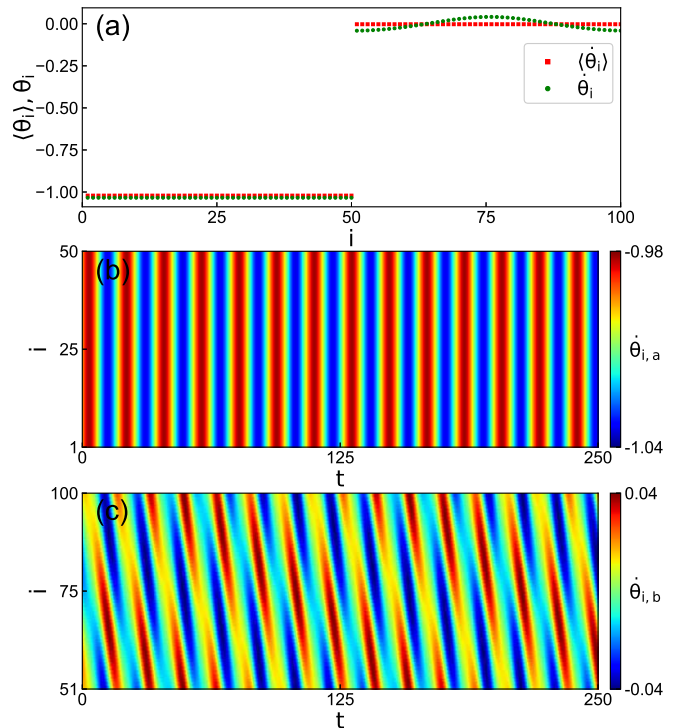


FIG. 2: (color online). Dynamical behaviours in the two groups  $a$  and  $b$ . (a) The distributions of effective frequencies  $\langle\dot{\theta}_i\rangle$  (red “squares”) and instantaneous frequencies  $\dot{\theta}_i(t)$  (green “points”) where the index with  $i \in [1, 50]$  represent the group  $a$  and that with  $i \in [51, 100]$  denote the group  $b$ . (b) and (c) show the evolutions of  $\dot{\theta}_i(t)$  for the groups  $a$  and  $b$ , respectively.

try [66]. This synchronization in the whole region of initial conditions of group  $b$  destroys its two states property and thus destroys the complementary feature between the two groups or the robustness of CS. (ii) Comparing Fig. 3(c) with Fig. 1(c) one can see that the region of non-synchronization in Fig. 3(c) is increased and its value of  $R_a$  is larger than that in Fig. 1(c), indicating that the asymmetric couplings reduce the contrast ratio between the states of synchronization and non-synchronization in CS. These two points make the region of the attractor “S” be significantly increased.

So far, we have fixed the average initial phase difference as  $\Delta\Phi(0) = \frac{\pi}{4}$ . However, we find that the value of  $\Delta\Phi(0)$  will also influence the region of the attractor “S”. Let us take the group  $a$  as an example. Fig. 4(a) and (b) show the phase diagrams of  $R_a$  for  $\Delta\Phi(0) = 0$  and  $\frac{2\pi}{3}$ , respectively, where the other parameters are fixed the same as in Fig. 3(c). Comparing Fig. 4(a) with (b) and also comparing them with Fig. 3(c), one can see that their regions of the attractor “S” are largely different each other, indicating the key role of  $\Delta\Phi(0)$  in the region of the attractor “S”.

In sum, the robustness of chimera states with respect to initial conditions is only reflected in 2D slice of  $R_a(0)$  and  $R_b(0)$  for all the cases of Fig. 1(c) and (d), Fig. 3(c) and (d) and Fig. 4(a)-(d). Considering that the initial condition space is

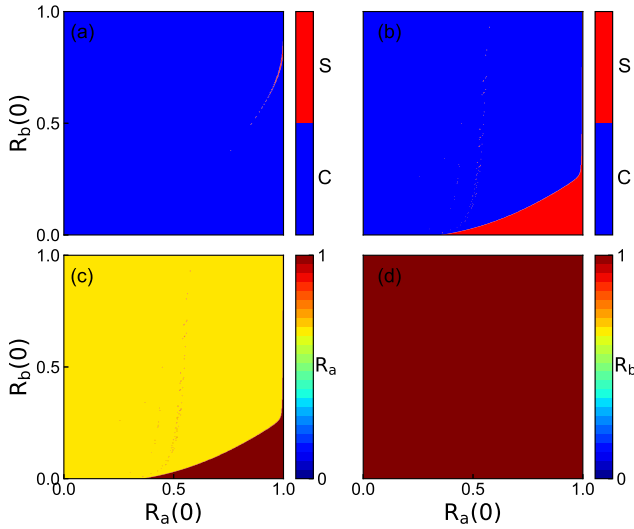


FIG. 3: (color online). (a) The synchronized region “S” for the case of symmetric coupling, corresponding to Fig. 1(c) and (d). (b) The synchronized region “S” for the case of asymmetric coupling with  $c_{ab} = 0.1$  and  $c_{ba} = 1.0$ . (c) and (d) represent the phase diagrams of  $R_a$  and  $R_b$  corresponding to (b), respectively. We have  $\Delta\Phi(0) = \frac{\pi}{4}$  for all these cases.

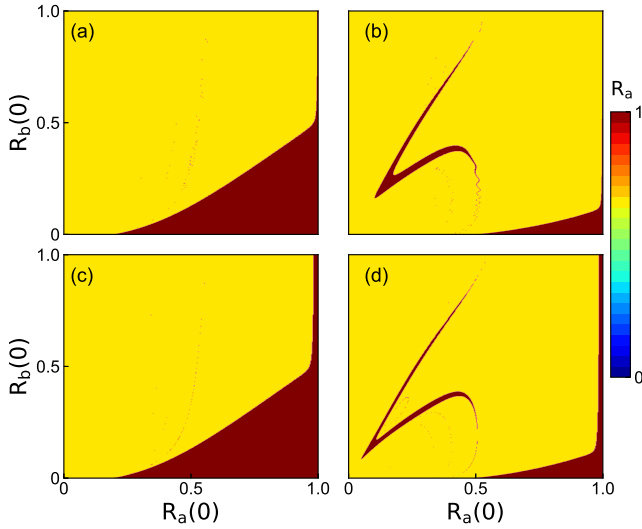


FIG. 4: (color online). Influence of the average initial phase difference in the group a. (a) and (b) represent the region of the attractor “S” for the case of asymmetric coupling with  $\Delta\Phi(0) = 0$  and  $\frac{2\pi}{3}$ , respectively. (c) and (d) represent the theoretical solutions corresponding to (a) and (b), respectively.

3D ( $R_a(0)$ ,  $R_b(0)$  and  $\Delta\Phi(0)$ ), it is better to also show this robustness to the third parameter  $\Delta\Phi(0)$ . For this purpose, we calculate the possibility  $P$  for the system to stay at the attractor “S” in the 2D plane of  $R_a(0)$  and  $R_b(0)$ . Instead of enumerating the diversity of the patterns “S”, it is maybe better to count the ratio  $P$  between the region of the attractor “S” and the total region including both the regions of “S” and “C”. That is,  $P$  will be proportional to the region of initial

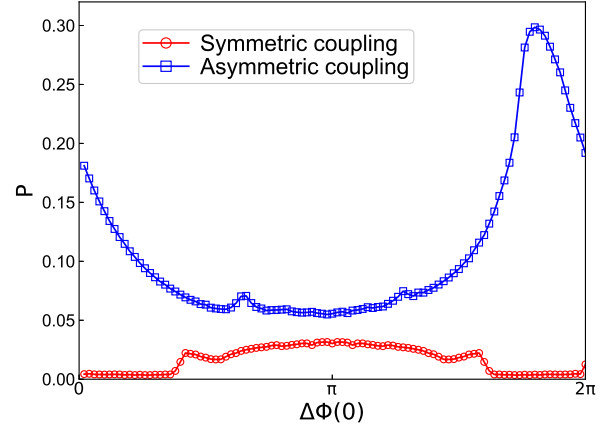


FIG. 5: (color online). Dependence of  $P$  on  $\Delta\Phi(0)$  where the initial conditions of  $R_a(0)$ ,  $R_b(0)$  are homogeneously distributed in  $(0, 1]$ . The red “circles” represent the case of symmetric coupling with  $c_{ab} = 1.0$  and  $c_{ba} = 1.0$ , while the blue “squares” denote the case of asymmetric coupling with  $c_{ab} = 0.1$  and  $c_{ba} = 1.0$ .

conditions which finally go to the attractor “S” [67, 68]. Fig. 5 shows how  $P$  changes with  $\Delta\Phi(0)$  where the red “circles” represent the case of symmetric coupling with  $c_{ab} = 1.0$  and  $c_{ba} = 1.0$  and the blue “squares” denote the case of asymmetric coupling with  $c_{ab} = 0.1$  and  $c_{ba} = 1.0$ . We see that (1)  $P$  depends on  $\Delta\Phi(0)$  and (2)  $P$  for the “squares” are larger than the corresponding  $P$  for the “circles”, indicating that asymmetric coupling enhance the transition from chimera state to synchronization.

Based on Figs. 3-5, we conclude that the region of the attractor “S” depends not only on the asymmetric couplings but also on the average initial phase difference. Moreover, we find that the phase lag parameter  $\alpha$  in Eq. (1) also influences the region of the attractor “S”. The left panels of Fig. 6, i.e. (a), (c), (e) and (g), show the patterns of “S” in the phase diagram of  $\Delta\Phi(0)$  and  $\Delta R(0)$  for different  $c_{ab}$  and  $\alpha$ , with the limits of  $R_a(0) + R_b(0) = 1.0$  and  $c_{aa} = c_{bb} = 1.0$ ,  $c_{ba} = 1.0$ . We see that their patterns can be quite different, indicating the induced diversity of the attractor “S”.

We fix  $c_{aa} = c_{bb} = 1.0$ ,  $c_{ba} = 1.0$  and let  $c_{ab}$  change. For each  $c_{ab}$ , we let  $R_a(0)$ ,  $R_b(0)$  change in  $(0, 1]$  and let  $\Delta\Phi(0)$  change in  $(0, 2\pi]$ . Fig. 7(a) shows the dependence of  $P$  on  $c_{ab}$  where the three curves represent the cases of  $\alpha = \frac{\pi}{2} - 0.1$ ,  $\alpha = \frac{\pi}{2} - 0.3$  and  $\alpha = \frac{\pi}{2} - 0.5$ , respectively. We see that with the increase of  $c_{ab}$ ,  $P$  is approximately decreased. Consider the fact that the increase of  $c_{ab}$  means a decrease of the difference between  $c_{ab}$  and  $c_{ba}$ . Thus, the increase of coupling asymmetry will result in a decrease of the robustness of CS, i.e. an increase of the region of the attractor “S”.

Thirdly, we consider the second kind of asymmetric couplings with  $c_{ab} = c_{ba}$  but  $c_{aa} \neq c_{bb}$ , i.e. non-symmetric inner-group couplings. In detail, we keep  $c_{ab} = c_{ba} = 1.0$  and  $c_{aa} = 1.0$ , but let  $c_{bb}$  change. We find the similar behaviours as that of the left panels of Fig. 6, i.e. the region of the attractor “S” can be also enhanced by the asymmet-

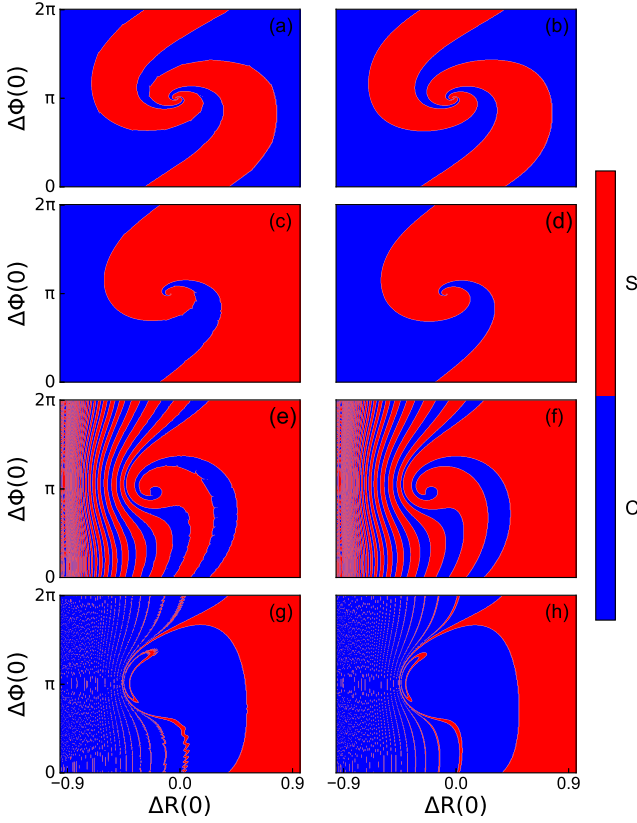


FIG. 6: (color online). Typical patterns of the attractor “S” on the phase diagram of  $\Delta\Phi(0)$  and  $\Delta R(0)$  for different pairs of  $c_{ab}$  and  $\alpha$ , with the limits of  $R_a(0) + R_b(0) = 1.0$  and  $c_{aa} = c_{bb} = 1.0, c_{ba} = 1.0$ . The left panels represent the numerical simulations, while the right panels represent the corresponding theoretical results. The parameters are as follows. (a) and (b):  $c_{ab} = 0.9$  and  $\alpha = \frac{\pi}{2} - 0.5$ ; (c) and (d):  $c_{ab} = 0.7$  and  $\alpha = \frac{\pi}{2} - 0.5$ ; (e) and (f):  $c_{ab} = 0.25$  and  $\alpha = \frac{\pi}{2} - 0.3$ ; (g) and (h):  $c_{ab} = 0.0822$  and  $\alpha = \frac{\pi}{2} - 0.1$ .

ric inner-group coupling. The left panels of Fig. 8, i.e. (a), (c), (e) and (g), shows the patterns of “S” on the phase diagram of  $\Delta\Phi(0)$  and  $\Delta R(0)$  for different  $c_{bb}$ , with the limits of  $R_a(0) + R_b(0) = 1.0$  and  $\alpha = \frac{\pi}{2} - 0.3$ . We see that the region of the attractor “S” also show a diversity of patterns. Therefore, the ratio  $P$  can be used to characterize the dependence of the region of the attractor “S” on  $c_{bb}$ . Fig. 7(b) shows the results where the three curves represent the cases of  $\alpha = \frac{\pi}{2} - 0.1, \alpha = \frac{\pi}{2} - 0.3$  and  $\alpha = \frac{\pi}{2} - 0.5$ , respectively. Comparing Fig. 7(b) with (a), we see that they are similar each other when  $c_{bb} < 2$ . However,  $P$  will be easy to reach unity when  $c_{bb} > 2$ , indicating that a strong degree of asymmetric inner-group coupling will destroy the robustness of CS.

### III. THEORETICAL ANALYSIS

To conveniently analyze the collective dynamics, Ott and Antonsen presented an approach to significantly reduce the dimension of globally coupled oscillators [69, 70], resulting in the low dimensional behavior of system. We here adopt this

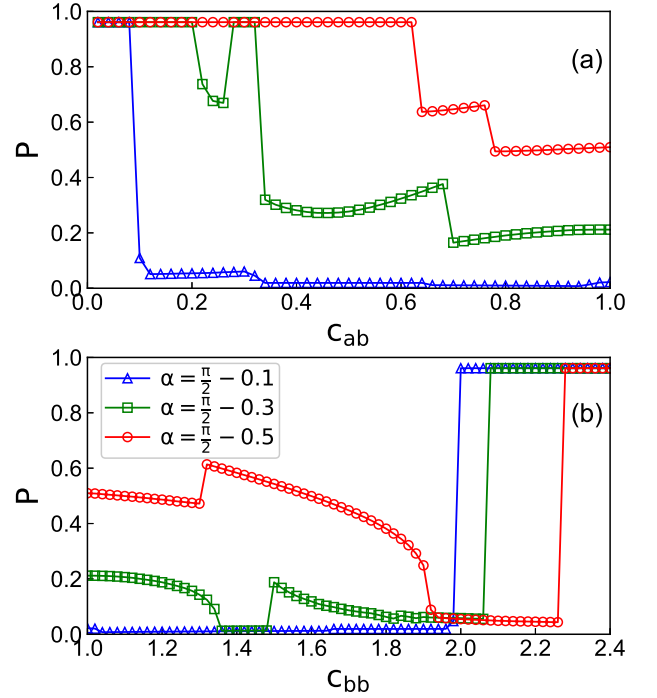


FIG. 7: (color online). The diversity of the patterns “S” induced by the asymmetric couplings. (a)  $P$  versus  $c_{ab}$  for the case of asymmetric inter-group couplings with fixed  $c_{aa} = c_{bb} = 1.0$  and  $c_{ba} = 1.0$ . (b)  $P$  versus  $c_{bb}$  for the case of asymmetric inner-group couplings with fixed  $c_{aa} = 1.0$  and  $c_{ab} = c_{ba} = 1.0$ . The initial values of  $R_a(0), R_b(0)$  are homogeneously taken from  $(0, 1]$  and  $\Delta\Phi(0)$  from  $(0, 2\pi]$ .

idea to analyze the coexistence of the attractor “S” and the attractor “C”. In the thermodynamical limit, the state of the oscillator system at time  $t$  can be described by a continuous distribution function,  $f(\theta, \omega, t)$ . Taking the group  $a$  of system (1) as an example, its continuity equation is as follows

$$\frac{\partial f_a}{\partial t} + \frac{\partial(v_a f_a)}{\partial \theta} = 0, \quad (4)$$

where  $f_a(\theta_a, \omega_a, t)$  is the distribution function at time  $t$  and phase  $\theta$  of an oscillator.  $v_a(\theta_a, \omega_a, t)$  is its angular velocity and can be defined as

$$\begin{aligned} v_a = & \omega_a \\ & + R_a c_{aa} \int_0^{2\pi} \int_{-\infty}^{\infty} \sin(\theta'_a - \theta_a - \alpha) f_a(\theta'_a, \omega'_a, t) d\theta'_a d\omega'_a \\ & + R_a c_{ab} \int_0^{2\pi} \int_{-\infty}^{\infty} \sin(\theta_b - \theta_a - \alpha) f_b(\theta_b, \omega_b, t) d\theta_b d\omega_b. \end{aligned} \quad (5)$$

Let us introduce a complex order parameter  $z$ , defined as

$$z_a = R_a e^{i\Phi_a} = \int_0^{2\pi} \int_{-\infty}^{\infty} e^{i\theta_a} f_a(\theta_a, \omega_a, t) d\theta_a d\omega_a, \quad (6)$$

$$z_b = R_b e^{i\Phi_b} = \int_0^{2\pi} \int_{-\infty}^{\infty} e^{i\theta_b} f_b(\theta_b, \omega_b, t) d\theta_b d\omega_b. \quad (7)$$

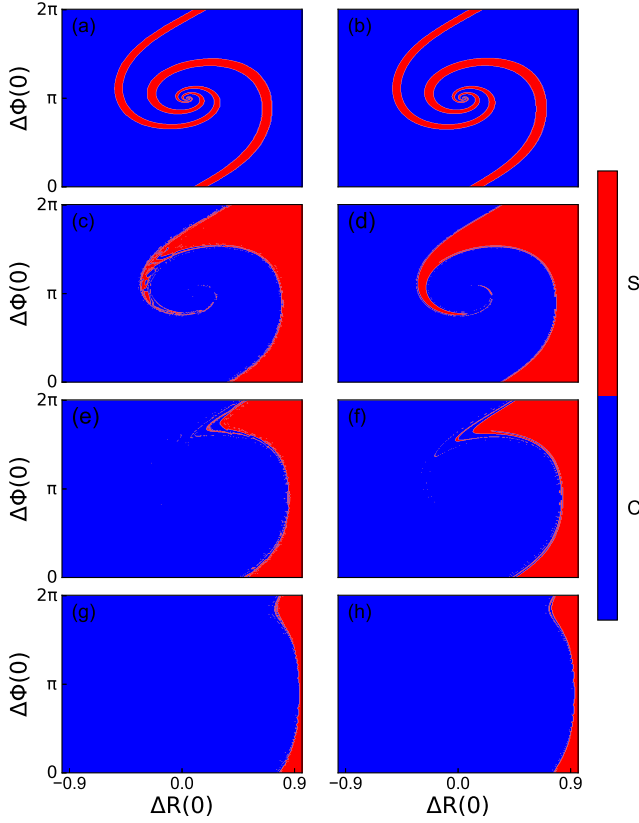


FIG. 8: (color online). Typical patterns of the region of the attractor “S” on the phase diagram of  $\Delta\Phi(0)$  and  $\Delta R(0)$  for different  $c_{bb}$ , with the limits of  $R_a(0) + R_b(0) = 1.0$  and  $\alpha = \frac{\pi}{2} - 0.3$ . The left panels represent the numerical simulations, while the right panels represent the corresponding theoretical results. The parameters are as follows. (a) and (b):  $c_{bb} = 1.2$ ; (c) and (d):  $c_{bb} = 1.5$ ; (e) and (f):  $c_{bb} = 1.56$ ; (g) and (h):  $c_{bb} = 2.0$ .

where  $R_a$  and  $R_b$  represent the order parameters of the groups  $a$  and  $b$ , respectively. Then,  $v_a(\theta_a, \omega_a, t)$  can be simplified into

$$v_a(\theta_a, \omega_a, t) = \omega_a + \frac{R_a c_{aa}}{2i} [z_a e^{-i\theta_a} e^{-i\alpha} - z_a^* e^{i\theta_a} e^{i\alpha}] + \frac{R_a c_{ab}}{2i} [z_b e^{-i\theta_a} e^{-i\alpha} - z_b^* e^{i\theta_a} e^{i\alpha}]. \quad (8)$$

According to the Ott-Antonsen ansatz [69, 70], the distribution  $f_a(\theta_a, \omega_a, t)$  can be written as a Fourier series in the form

$$f_a(\theta_a, \omega_a, t) = \frac{g_a(\omega_a)}{2\pi} \{1 + [\sum_{n=1}^{\infty} [h_a(\omega_a, t) e^{i\theta_a}]^n + c.c.]\}, \quad (9)$$

where the  $c.c.$  stands for complex conjugate. Substituting Eqs.(8) and (9) into Eq. (4) and doing the same derivation

as Ref. [31], we obtain

$$\begin{aligned} \dot{R}_a &= \frac{R_a - R_a^3}{2} [c_{aa} R_a \cos \alpha + c_{ab} R_b \cos(\Phi_a - \Phi_b + \alpha)], \\ \dot{\Phi}_a &= \omega_0 - \frac{(1 + R_a^2)}{2} \\ &\quad \times [c_{aa} R_a \sin \alpha + c_{ab} R_b \sin(\Phi_a - \Phi_b + \alpha)]. \end{aligned} \quad (10)$$

Similarly, we have the equations of order parameter for the group  $b$  as

$$\begin{aligned} \dot{R}_b &= \frac{R_b - R_b^3}{2} [c_{bb} R_b \cos \alpha + c_{ba} R_a \cos(\Phi_b - \Phi_a + \alpha)], \\ \dot{\Phi}_b &= \omega_0 - \frac{(1 + R_b^2)}{2} \\ &\quad \times [c_{bb} R_b \sin \alpha + c_{ba} R_a \sin(\Phi_b - \Phi_a + \alpha)]. \end{aligned} \quad (11)$$

Eqs. (10) and (11) are our theoretical results.

We now let  $\omega_0 = 0$  and use Eqs. (10) and (11) to confirm the above numerical simulations. We first go to the cases of Fig. 4(a) and (b) and use their corresponding parameters to solve the Eqs. (10) and (11). Fig. 4(c) and (d) show the results. Comparing Fig. 4(c) and (d) with their corresponding numerical results of Fig. 4(a) and (b), respectively, we see that Fig. 4(c) is very similar to Fig. 4(a) and Fig. 4(d) is very similar to Fig. 4(b), indicating that the theoretical results and numerical simulations have confirmed each other.

Then, we use the theoretical Eqs. (10) and (11) to the cases of Fig. 6(a), (c), (e) and (g) by taking their corresponding parameters. Fig. 6(b), (d), (f) and (h) show the results. Comparing them with their corresponding numerical results of Fig. 6(a), (c), (e) and (g), respectively, we see their highly consistency, indicating again that the theoretical results and numerical simulations have confirmed each other. Similarly, Fig. 8(b), (d), (f) and (h) show the theoretical results corresponding to Fig. 8(a), (c), (e) and (g), respectively. Once again, they are consistent with each other.

Moreover, to understand the transition from chimera state to synchronization better, we would like to make a further analysis on the dependence of synchronization on the parameters by following Refs. [31] and [68]. Letting  $\psi = \Phi_a - \Phi_b$  and  $\omega_0 = 0$ , Eqs. (10) and (11) can be combined into

$$\begin{aligned} \dot{R}_a &= \frac{R_a - R_a^3}{2} [c_{aa} R_a \cos \alpha + c_{ab} R_b \cos(\alpha + \psi)], \\ \dot{R}_b &= \frac{R_b - R_b^3}{2} [c_{bb} R_b \cos \alpha + c_{ba} R_a \cos(\alpha - \psi)], \\ \dot{\psi} &= -\frac{1 + R_a^2}{2} [c_{aa} R_a \sin \alpha + c_{ab} R_b \sin(\alpha + \psi)] \\ &\quad + \frac{1 + R_b^2}{2} [c_{bb} R_b \sin \alpha + c_{ba} R_a \sin(\alpha - \psi)] \end{aligned} \quad (12)$$

For a synchronized solution of Eq. (12), we have  $R_a = R_b = 1$ , which corresponds to the fixed point of  $\dot{R}_a = 0$ ,  $\dot{R}_b = 0$ , and  $\dot{\psi} = 0$ . We pay attention to the case of asymmetric coupling, which may come from either inter-group coupling  $c_{ab} \neq c_{ba}$  or inner-group coupling  $c_{aa} \neq c_{bb}$ .

In the case of  $c_{ab} \neq c_{ba}$ , we consider  $c_{aa} = c_{bb} = 1$  and  $c_{ba} = 1$  as an example. From the third equation Eq. (12) we have

$$\psi_0 = \alpha - \arctan \left[ \frac{\sin(2\alpha)c_{ab}}{\cos(2\alpha)c_{ab} + 1} \right]. \quad (13)$$

Thus, the fixed point of synchronized solution  $(1, 1, \psi_0)$  depends on the asymmetric parameter  $c_{ab}$  and the parameter  $\alpha$ . For simplicity, we denote  $SS_{\psi_0}$  as the fixed point. To analyze the stability of the fixed point, we check the Jacobian matrix of Eq. (12)

$$M = \begin{pmatrix} a_1 & a_2 & a_3 \\ b_1 & b_2 & b_3 \\ c_1 & c_2 & c_3 \end{pmatrix} \quad (14)$$

where

$$\begin{aligned} a_1 &= \frac{1}{2}(-3R_a^2 + 1)[c_{aa}R_a \cos \alpha + c_{ab}R_b \cos(\psi + \alpha)] + \\ &\quad \frac{1}{2}(-R_a^3 + R_a)c_{aa} \cos \alpha \\ a_2 &= \frac{1}{2}(-R_a^3 + R_a)c_{ab} \cos(\psi + \alpha) \\ a_3 &= -\frac{1}{2}(-R_a^3 + R_a)c_{ab}R_b \sin(\psi + \alpha) \\ b_1 &= \frac{1}{2}(-R_b^3 + R_b)c_{ba} \cos(\alpha - \psi) \\ b_2 &= \frac{1}{2}(-3R_b^2 + 1)[c_{bb}R_b \cos \alpha + c_{ba}R_a \cos(\alpha - \psi)] + \\ &\quad \frac{1}{2}(-R_b^3 + R_b)c_{bb} \cos \alpha \\ b_3 &= \frac{1}{2}(-R_b^3 + R_b)c_{ba}R_a \sin(\alpha - \psi) \\ c_1 &= -R_a[c_{aa}R_a \sin \alpha + c_{ab}R_b \sin(\psi + \alpha)] - \\ &\quad \frac{1}{2}(R_a^2 + 1)c_{aa} \sin \alpha + \frac{1}{2}(R_b^2 + 1)c_{ba} \sin(\alpha - \psi) \\ c_2 &= -\frac{1}{2}(R_a^2 + 1)c_{ab} \sin(\psi + \alpha) + R_b[c_{bb}R_b \sin \alpha + \\ &\quad c_{ba}R_a \sin(\alpha - \psi)] + \frac{1}{2}(R_b^2 + 1)c_{bb} \sin \alpha \\ c_3 &= -\frac{1}{2}(R_a^2 + 1)c_{ab}R_b \cos(\psi + \alpha) - \\ &\quad \frac{1}{2}(R_b^2 + 1)c_{ba}R_a \cos(\alpha - \psi) \end{aligned} \quad (15)$$

Substituting the fixed point into (15), we obtain the eigenvalues of (14) as

$$\lambda_{1,2,3} = \begin{cases} -c_{aa} \cos \alpha - c_{ab} \cos(\psi + \alpha) \\ -c_{bb} \cos \alpha - c_{ba} \cos(\alpha - \psi) \\ -c_{ab} \cos(\psi + \alpha) - c_{ba} \cos(\alpha - \psi) \end{cases} \quad (16)$$

The synchronized solution  $SS_{\psi_0}$  will be stable when the maximum of the three eigenvalues of (16) is negative; otherwise, it will be unstable. Fig. 9(a) shows the results where the red and blue points represent the stable and unstable regions, respectively. It is easy to notice that the chimera state exists only when  $\alpha$  is around  $\pi/2$ .

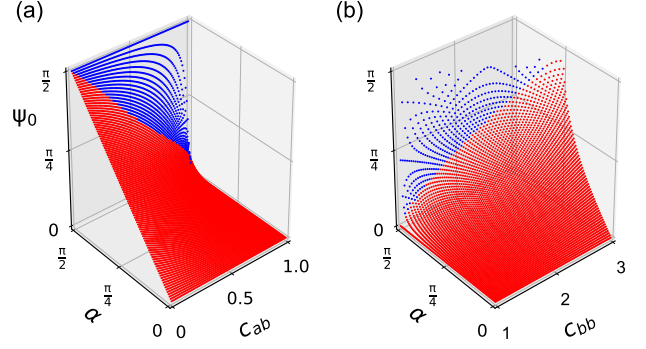


FIG. 9: (color online). Stability analysis of the synchronized solution  $SS_{\psi_0}$  where the red and blue points represent the stable and unstable regions, respectively. (a) Case of  $c_{ab} \neq c_{ba}$ ; and (b) case of  $c_{aa} \neq c_{bb}$ .

In the case of  $c_{aa} \neq c_{bb}$ , we consider  $c_{ab} = c_{ba} = 1$  and  $c_{aa} = 1$  as an example. From the third equation Eq. (12) we have

$$\psi_0 = \arcsin \left[ \frac{\sin \alpha (c_{bb} - 1)}{2 \cos \alpha} \right] \quad (17)$$

Fig. 9(b) shows the dependence of the synchronized solution  $SS_{\psi_0}$  on the parameters  $\alpha$  and  $c_{bb}$  where the red and blue points represent the stable and unstable regions, respectively. It confirms again that the chimera state exists only when  $\alpha$  is around  $\pi/2$ .

Finally, we discuss the bifurcation diagram of chimera state by following Refs. [31] and [68]. We take the case of synchronized group b and unsynchronized group a as an example, i.e.  $R_b = 1$  and  $0 < R_a < 1$ . By  $\dot{R}_a = 0$  we obtain

$$c_{aa}R_a \cos \alpha + c_{ab}R_b \cos(\psi + \alpha) = 0 \quad (18)$$

In the case of  $c_{ab} \neq c_{ba}$ , we consider  $c_{aa} = c_{bb} = 1$  and  $c_{ba} = 1$ , which gives

$$R_a = -\frac{c_{ab} \cos(\psi + \alpha)}{\cos \alpha} \quad (19)$$

By  $\dot{\psi} = 0$  we have

$$c_{ab} = -\frac{\sin(\alpha)R_a^3 + R_a \sin \alpha - 2R_a \sin(\alpha - \psi) - 2 \sin \alpha}{(R_a^2 + 1) \sin(\psi + \alpha)} \quad (20)$$

To obtain the saddle-node bifurcation, the sub-Jacobian matrix of Eq. (12) must satisfy

$$\Delta = \begin{vmatrix} a_1 & a_3 \\ c_1 & c_3 \end{vmatrix} = 0 \quad (21)$$

To obtain the Hopf bifurcation, the trace of (21) must satisfy

$$T = a_1 + c_3 = 0 \quad (22)$$

Sweeping  $\alpha$  and  $\psi$  yields the corresponding  $R_a$  and  $c_{ab}$ . Furthermore, we calculate the probability for chimera state by

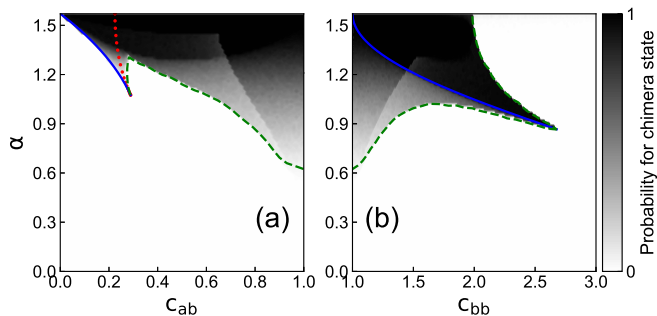


FIG. 10: (color online). Bifurcation diagram for chimera states where the dotted red, solid blue and dashed green lines represent Hopf, saddle-node and homoclinic bifurcations, respectively. (a) Case of  $c_{ab} \neq c_{ba}$ ; and (b) case of  $c_{aa} \neq c_{bb}$ . The probabilities for chimera states are measured by realizing 1000 random initial conditions for each set of parameters.

realizing 1000 random initial conditions for each set of parameters. Fig. 10(a) shows the results.

In the case of  $c_{aa} \neq c_{bb}$ , we consider  $c_{ab} = c_{ba} = 1$  and  $c_{aa} = 1$ . By doing the same process as in Fig. 10(a) we obtain Fig. 10(b). From both Fig. 10(a) and (b) we see that the asymmetric coupling increases the transition from chimera state to synchronization.

#### IV. DISCUSSIONS AND CONCLUSIONS

The interesting of CS comes from its counterintuitive coexistence of coherent and incoherent oscillations in populations of identical oscillators where we can traditionally only expect either a complete synchronization or an unsynchronized state. Since the finding of CS in 2002 [14], most of the attention has been paid to its conditions and its diversity [36, 71], while little attention has been paid to the relationship between the attractor “S” and the attractor “C”. We here show that for the symmetric coupled populations, the basin of the attractor “S” is ignorable in the phase diagram of initial conditions (see Fig. 3(a) for example), which implies that it is not very necessary to pay attention to the attractor “S” and thus no necessary to discuss the relationship between the attractor “S” and the attractor “C”.

However, in realistic situations, the couplings are generally asymmetric. Take the human beings as an examples, which was shown to have a first-night effect [72], i.e. a kind of CS for the unihemispheric sleep in the first night of traveling hotel. It is well known that the left and right hemispheres of the brain are taking different functions with asymmetric cou-

plings between them. Thus, it is very necessary to study how the asymmetric couplings influence the relationship between the attractor “S” and the attractor “C”, which is just done in this work. We interestingly find that the asymmetric couplings do influence the basins of both the attractor “S” and the attractor “C” in the phase diagram of initial conditions and result in the diversity of patterns for the attractor “S”, which may have applications in controlling of CS.

This asymmetry enhanced synchronization can be further understood as follows. For the classical model of two coupled groups in [31], its chimera state depends sensitively on the chosen initial conditions. In other words, its synchronization can be easily observed by randomly chosen initial conditions. Thus, it is not very interesting to study its enhanced synchronization. But for the adaptive model (1), its chimera state has robustness because of the control of local order parameters. Take the asymmetric case of  $c_{ab} \neq c_{ba}$  as an example. When  $c_{ab} = c_{ba}$ , every oscillator in the two groups will be in the same position. In this case, the local order parameters in (1) will try to keep their local behaviours and thus results in the robustness. However, when  $c_{ab} \neq c_{ba}$ , the oscillators in one group will have different positions than that in the other group. Suppose  $c_{ab} > c_{ba}$ . We divide  $c_{ab}$  into two parts, i.e.  $c_{ab} = c_{ba} + (c_{ab} - c_{ba})$ . The part of  $c_{ba}$  will contribute a mean-field to every oscillator in the system, while the part of  $(c_{ab} - c_{ba})$  will contribute a perturbation. This perturbation will kick the oscillators out of their local states and thus enhance the synchronization between the two groups. This synchronization mechanism has been confirmed in both the symmetry breaking system [66] and weighted networks [11].

In conclusion, we have presented an adaptive model to describe both the robustness of CS and the relationship between the attractor “S” and the attractor “C”. We find that in the case of symmetric couplings, the two groups may easily go to different final states and thus show a robustness of CS. More interestingly, we study two kinds of asymmetric couplings and show that there is a finite probability for the two groups to go to the attractor “S”, i.e. partially destroying the robustness of CS. No matter it is the asymmetric inter-group couplings or the asymmetric inner-group couplings, we reveal that both of them can show the diversity of patterns for the attractor “S” in the phase diagram of initial conditions. Moreover, a theoretical analysis of dimension reduction is provided to explain the numerical simulations.

This work was partially supported by the NNSF of China under Grant Nos. 11375066 and 11675056, 973 Program under Grant No. 2013CB834100, and the NSF of Guizhou Province Education Department under Grant No. KY[2014]316.

[1] J. A. Acebron, L. L. Bonilla, C. J. P. Vicente, F. Ritort, and R. Spigler, *Rev. Mod. Phys.* **77**, 137 (2005).  
 [2] S. Boccaletti, V. Latora, and Y. Moreno, *Phys. Rep.* **424**, 175 (2006).  
 [3] A. Arenas, A. Diaz-Guilera, J. Kurths, Y. Moreno, and C. Zhou,

*Phys. Rep.* **469**, 93 (2008).  
 [4] S. Boccaletti, J. A. Almendral, S. Guan, I. Leyva, Z. Liu, I. Sendiña-Nadal, and Y. Zou, *Phys. Rep.* **660**, 1 (2016).  
 [5] P. S. Skardal, D. Taylor, and J. Sun, *Phys. Rev. Lett.* **113**, 144101 (2014).

- [6] L. F. Lago-Fernández, R. Huerta, F. Corbacho, and J. A. Sigüenza, *Phys. Rev. Lett.* **84**, 2758 (2000).
- [7] M. Barahona and L. M. Pecora, *Phys. Rev. Lett.* **89**, 054101 (2002).
- [8] J. Gómez-Gardeñes, S. Gómez, A. Arenas, and Y. Moreno, *Phys. Rev. Lett.* **106**, 128701 (2011).
- [9] I. Sendiña-Nadal, I. Leyva, A. Navas, J. A. Villacorta-Atienza, J. A. Almendral, Z. Wang, and S. Boccaletti, *Phys. Rev. E* **91**, 032811 (2015).
- [10] M. Chavez, D. U. Hwang, A. Amann, H. G. E. Hentschel, and S. Boccaletti, *Phys. Rev. Lett.* **94**, 218701 (2005).
- [11] C. Zhou, A. E. Motter, and J. Kurths, *Phys. Rev. Lett.* **96**, 034101 (2006).
- [12] C. Zhou, L. Zemanov, G. Zamora, C. C. Hilgetag, and J. Kurths, *Phys. Rev. Lett.* **97**, 238103 (2006).
- [13] X. Zhang, S. Boccaletti, S. Guan, and Z. Liu, *Phys. Rev. Lett.* **114**, 038701 (2015).
- [14] Y. Kuramoto and D. Battogtokh, *Nonlin. Phenom. Complex Syst.* **5**, 380 (2002).
- [15] D. M. Abrams and S. H. Strogatz, *Phys. Rev. Lett.* **93**, 174102 (2004).
- [16] E. Omel'chenko, Y. L. Maistrenko, and P. A. Tass, *Phys. Rev. Lett.* **100**, 044105 (2008).
- [17] G. C. Sethia, A. Sen, and F. M. Atay, *Phys. Rev. Lett.* **100**, 144102 (2008).
- [18] G. Bordyugov, A. Pikovsky, and M. Rosenblum, *Phys. Rev. E* **82**, 035205 (2010).
- [19] M. J. Panaggio and D. M. Abrams, *Phys. Rev. Lett.* **110**, 094102 (2013).
- [20] C. R. Laing, *Physica (Amsterdam) D* **238**, 1569 (2009); *Chaos* **19**, 013113 (2009).
- [21] E. A. Martens, C. R. Laing, and S. H. Strogatz, *Phys. Rev. Lett.* **104**, 044101 (2010).
- [22] M. Wolfrum, O. E. Omel'chenko, S. Yanchuk, and Y. L. Maistrenko, *Chaos* **21**, 013112 (2011).
- [23] C. R. Laing, K. Rajendran, and I. G. Kevrekidis, *Chaos* **22**, 013132 (2012).
- [24] Y. Zhu, Y. Li, M. Zhang, and J. Yang, *Europhys. Lett.* **97**, 10009 (2012).
- [25] D. Dudkowski, Y. Maistrenko, and T. Kapitaniak, *Phys. Rev. E* **90**, 032920 (2014).
- [26] I. Omelchenko, A. Provata, J. Hizanidis, E. Schöll, and P. Hövel, *Phys. Rev. E* **91**, 022917 (2015).
- [27] P. Jaros, Y. Maistrenko, and T. Kapitaniak, *Phys. Rev. E* **91**, 022907 (2015).
- [28] F. Böhm, A. Zakharova, E. Schöll, and K. Lüdge, *Phys. Rev. E* **91**, 040901 (2015).
- [29] N. C. Rattenborg, C. J. Amlaner, and S. L. Lima, *Neurosci. Biobehav. Rev.* **24**, 817 (2000).
- [30] C. G. Mathews, J. A. Lesku, S. L. Lima, and C. J. Amlaner, *Ethology* **112**, 286 (2006).
- [31] D. M. Abrams, R. Mirollo, S. H. Strogatz, and D. A. Wiley, *Phys. Rev. Lett.* **101**, 084103 (2008).
- [32] A. Pikovsky and M. Rosenblum, *Phys. Rev. Lett.* **101**, 264103 (2008).
- [33] R. Ma, J. Wang, and Z. Liu, *Europhys. Lett.* **91**, 40006 (2010).
- [34] I. Omelchenko, E. Omel'chenko, P. Hövel, and E. Schöll, *Phys. Rev. Lett.* **110**, 224101 (2013).
- [35] J. Hizanidis, V. G. Kanas, A. Bezerianos, and T. Bountis, *T. Inter. J. Bif. and Chaos* **24**, 1450030 (2014).
- [36] C. Tian, X. Zhang, Z. Wang, and Z. Liu, *Front. Phys.* **12**, 128904 (2017).
- [37] H. Sakaguchi, *Phys. Rev. E* **73**, 031907 (2006).
- [38] S. Olmi, A. Politi, and A. Torcini, *Europhys. Lett.* **92**, 60007 (2010).
- [39] I. Omelchenko, Y. Maistrenko, P. Hövel, and E. Schöll, *Phys. Rev. Lett.* **106**, 234102 (2011).
- [40] I. Omelchenko, B. Riemenschneider, P. Hövel, Y. Maistrenko, and E. Schöll, *Phys. Rev. E* **85**, 026212 (2012).
- [41] C. Gu, G. St-Yves, and J. Davidsen, *Phys. Rev. Lett.* **111**, 134101 (2013).
- [42] M. J. Panaggio and D. M. Abrams, *Phys. Rev. E* **91**, 022909 (2015).
- [43] O. E. Omel'chenko, M. Wolfrum, S. Yanchuk, Y. L. Maistrenko, and O. Sudakov, *Phys. Rev. E* **85**, 036210 (2012).
- [44] J. Xie, E. Knobloch, and H. C. Kao, *Phys. Rev. E* **92**, 042921 (2015).
- [45] Y. Maistrenko, O. Sudakov, O. Osiv, and V. Maistrenko, *New J. Phys.* **17**, 073037 (2015).
- [46] E. A. Martens, C. R. Laing, and S. H. Strogatz, *Phys. Rev. Lett.* **104**, 044101 (2010).
- [47] A. M. Hagerstrom, T. E. Murphy, R. Roy, P. Hövel, I. Omelchenko, and E. Schöll, *Nat. Phys.* **8**, 658 (2012).
- [48] M. R. Tinsley, S. Nkomo, and K. Showalter, *Nat. Phys.* **8**, 662 (2012).
- [49] E. A. Viktorov, T. Habruseva, S. P. Hegarty, G. Huyet, and B. Kelleher, *Phys. Rev. Lett.* **112**, 224101 (2014).
- [50] M. Wickramasinghe and I. Z. Kiss, *Phys. Chem. Chem. Phys.* **16**, 18360 (2014).
- [51] E. A. Martens, S. Thutupalli, A. Fourrière, and O. Hallatschek, *Proc. Natl. Acad. Sci.* **110**, 10563(2013).
- [52] L. Larger, B. Penkovsky, and Y. Maistrenko, *Phys. Rev. Lett.* **111**, 1(2013).
- [53] K. Schöenleber, C. Zensen, A. Heinrich, and K. Krischer, *New J. Phys.* **16**, 63024 (2014).
- [54] E. M. Cherry and F. H. Fenton, *New J. Phys.* **10**, 125016 (2008).
- [55] J. M. Davidenko and A. V. Pertsov, *Nature* **355**, 349 (1992).
- [56] R. A. Gray, A. M. Pertsov, and J. Jalife, *Nature* **392**, 75 (1998).
- [57] R. A. Gray and N. Chattipakorn, *Proc. Natl. Acad. Sci.* **102**, 4672 (2005).
- [58] R. Cossart, D. Aronov, and R. Yuste, *Nature* **423**, 283 (2003).
- [59] K. E. Poskanzer and R. Yuste, *Proc. Natl. Acad. Sci.* **108**, 18453 (2011).
- [60] A. Luczak, P. Barthó, S. L. Marguet, G. Buzsáki, and K.D. Harris, *Proc. Natl. Acad. Sci.* **104**, 347 (2007).
- [61] X. Zhang, H. Bi, S. Guan, J. Liu, and Z. Liu, *Phys. Rev. E* **94**, 012204 (2016).
- [62] P. McCullagh, *The Annals of Statistics* **24**, 787 (1996).
- [63] H. Bi, X. Hu, S. Boccaletti, X. Wang, Y. Zou, Z. Liu, and S. Guan, *Phys. Rev. Lett.* **117**, 204101 (2016).
- [64] W. Zhou, Y. Zou, J. Zhou, Z. Liu, and S. Guan, *Chaos* **26**, 123117 (2016).
- [65] T. Qiu, S. Boccaletti, I. Bonamassa, Y. Zou, J. Zhou, Z. Liu, and S. Guan, *Sci. Rep.* **6**, 36713 (2016).
- [66] T. Nishikawa and A. E. Motter, *Phys. Rev. Lett.* **117**, 114101 (2016).
- [67] D. A. Wiley, S. H. Strogatz, and M. Girvan, *Chaos* **16**, 015103 (2006).
- [68] E. A. Martens, M. J. Panaggio, and D. M. Abrams, *New J. Phys.* **18**, 022002 (2016).
- [69] E. Ott and T. M. Antonsen, *Chaos* **18**, 037113 (2008).
- [70] E. Ott and T. M. Antonsen, *Chaos* **19**, 023117(2009).
- [71] M. J. Panaggio and D. M. Abrams, *Nonlinearity* **28**, R67 (2015).
- [72] M. Tamaki, J. W. Bang, T. Watanabe, and Y. Sasaki, *Curr. Biol.* **26**,1190 (2016).